Comparison of two contact models in the simulation of friction stir welding process

Z. Zhang

Abstract Two contact models are used to simulate the thermo-mechanical interaction process in friction stir welding. Comparison shows that the classical Coulomb friction model can be accurate enough for the simulation of friction stir welding in lower angular velocity. But in higher angular velocity, the classical Coulomb friction model fails to work due to the increase of the dynamic effect of the welding tool. Because the shear failure of material is considered in modified Coulomb friction model, the increase of the frictional stress on the tool–plate interface is limited by the shear failure. So, this model can keep valid even when the angular velocity of the welding tool is increased to a high level.

Introduction

Friction stir welding (FSW) was invented in 1991 by Thomas et al. at the Welding Institute in UK [1]. The main advantage of FSW over the traditional fusion joining techniques is that no melting occurs. So the defects in traditional fusion joining techniques can be minimized or eliminated, which makes FSW interesting for joining some hard-to-weld materials such as aluminum alloys, and magnesium alloys.

One of the main topics in the investigation on FSW is the temperature field in the FSW process. Although the temperature in FSW is lower than the melting points of the weld material, the temperature is still high enough for phase transformation [2]. The knowledge of the time–temperature history of the welds is needed to connect the weld hardness data to the welding parameters [3]. So it is very important for the studies on temperature variation in FSW. Usually the temperature in FSW is measured by using thermocouples [4, 5]. But it is very difficult for the investigation of temperature variation in the nugget zone by this measurement. In fact, numerical method can be very efficient and convenient for this study and has been used widely in the field of FSW. The modeling of heat transfer, fluid flow, and mass transfer can provide the detailed insight into the welding processes that could not have been obtained otherwise [6]. So many researches have been performed on the mass transfer and heat transfer in FSW to investigate its mechanism for joining.

Using the machine power input, heat source was calculated by Khandkar et al. [7] for the simulation of temperature variation in FSW. A thermal model was proposed by Mandal et al. [8] using hot channel approach to investigate the temperature distributions in FSW. Bastier et al. [9] used computational fluid dynamic method to investigate the material flow and temperature variations in FSW. A three-dimensional heat transfer model was presented by Song et al. [10] in which a moving coordinate was introduced for the modeling of the moving heat source. Schmidt et al. [11] presented a fully coupled thermo-mechanical model of FSW in which not only the temperature but also the material deformations can be investigated. All the above-mentioned models can predict the temperature variations with experimental validation. But these models cannot be directly used to investigate another main topic in the investigation on the nature of FSW—material transportations.

Z. Zhang (✉)
State Key Laboratory of Structural Analysis for Industrial Equipment, Department of Engineering Mechanics, Faculty of Vehicle Engineering and Mechanics, Dalian University of Technology, Dalian 116024, China
e-mail: zhangz@dlut.edu.cn

The investigation on material transportations in FSW is very important because it can answer the question on how the plates are joined using FSW. Guerra et al. [12] used a faying surface tracer and a nib frozen in place during welding to observe the material flows in FSW when a cylindrical pin was used. Colligan [13] used the steel shot tracer technique to visualize the material flow patterns in FSW. Material flows were also studied by Li et al. [14], Muthukumaran et al. [15], and Reynolds [16] through experiments. Compared to these studies with experiments, numerical method is more convenient to investigate the material transportations in FSW. Buffa et al. [17] used continuum-based FEM to simulate the friction stir welding process. While the temperature can be approximately symmetric to the welding line, the effective strain can keep non-symmetric. The three-dimensional viscoplatic flow and heat transfer in FSW of mild steel were investigated by Nandan et al. [18] in detail both experimentally and theoretically. The different material flows on the retreating side and the advancing side in 2D case are further studied by Zhang et al. [19]. Using the velocity field in FSW, material transportations are further studied in a 3D case [20]. Although the material flow patterns shown in these researches [19, 20] can be fitted well with the experimental observations [12–16], a limitation occurs. The temperature field is taken from experiments. To eliminate this limitation, Zhang et al. [21, 22] further developed a thermo-mechanical model to predict the temperature variations and material transportations in FSW. From the numerical modeling of FSW, it can be found that the temperature can be increased with the increase in the angular velocity of the welding tool [18]. Meanwhile, the computed results showed significant asymmetry of the temperature profiles around the welding tool in FSW [23].

FSW, as well as FSP (friction stir processing), is believed to be in solid state (FSP is a subfield of FSW [1] and has been studied by many researchers [24, 25]). This means that the temperature cannot be changed too much when the angular velocity is changed, which needs to be studied in detail with consideration of the contact models in FSW. A key point to determine the temperature simulation in FSW is the selection of the contact model in the tool–plate interface. Coulomb friction law is used by Schmidt et al. [11] and Zhang et al. [21, 22] in the coupled thermo-mechanical simulation of FSW. But in Coulomb friction law, the friction force in the tool–plate interface is directly determined by the friction coefficient and the contact pressure. In fact, the friction shear stress cannot be increased without upper limit because of the shear failure of the material. So, two contact models are adopted in the current work to investigate the heat generation and material transportations for comparisons. This work can help the

investigation on the physical nature of heat generation and can contribute to the numerical studies on FSW.

Model description

The welding plate made of AA6061-T6 is taken as a round plate with diameter of 80 mm to simulate the material transportations in the flow region near the tool–plate interface. The welding plate can be divided into two parts: inflow region and outflow region. The translational velocity, 2.363 mm/s, is applied to the inflow and outflow regions, which is equal to the welding speed of the welding tool in a real manufacture. A pressure of 70 MPa is applied on the shoulder. The welding plate is meshed into 10,500 elements consisting of 12,480 nodes. Reduced integration is used for higher computational efficiency. Hourglassing is controlled by stiffness method to avoid zero-energy of elements. The material properties, including the elastic modulus, yield function, Poisson ratio, are functions of temperature [19]. This is very important for a thermo-mechanical analysis in FSW, especially the yield function. When the material near the tool–plate interface is heated by friction and plastic deformation, the material in this region becomes softer and easier to stir.

The constitutive equation is as follows,

$$F_d\left(\sigma_{ij}, T\right) = \frac{1}{2}\sigma'_{ij}\sigma'_{ij} - \frac{1}{3}\sigma_s^2(T) = 0 \qquad (1)$$

$$D_p = \dot{\lambda}\frac{3\sigma'}{2\bar{\sigma}} \qquad (2)$$

where σ' denotes the deviatonic part of the Kirchhoff stress. σ_s is the yield stress which is the function of temperature T, as mentioned above. $\dot{\lambda}$ represents the inelastic flow rate. $\bar{\sigma}$ is the equivalent stress. D_p represents the inelastic rate of deformation.

The rotating tool is made of steel, which has a density of 7,800 kg/m^3. Due to the obvious difference between the welding plate and the welding tool, the later is considered as a rigid body. The radii of the shoulder and the pin are 9 and 3 mm, respectively.

The heat generated from friction is controlled by the following equation,

$$D_{fric} = \eta\tau\dot{\gamma} \qquad (3)$$

where D_{fric} is friction dissipation, τ is the friction stress on the tool–plate interface and $\dot{\gamma}$ is the slipping rate. η is the heat efficiency, which is taken as 95% in the current simulation.

The determination of the friction stress is different in the two contact models: Coulomb friction law and modified Coulomb friction law. In Coulomb friction law,

$$\tau_{\text{crit}} = \mu P \qquad (4)$$

where μ is the friction coefficient. P is the calculated contact pressure.

Defining the equivalent friction stress as follows,

$$\tau_{\text{eq}} = \sqrt{\tau_1^2 + \tau_2^2} \qquad (5)$$

when $\tau_{\text{eq}} = \tau_{\text{crit}}$, slip occurs. This slip can be accumulated until a steady state can be reached. In the initial start of FSW, the material on the welding plate is still and at the same time the welding tool is rotated with a certain angular velocity. A relative motion can be found and the heat generation can be calculated. From the material movements and temperature variations in Ref. [21], it can be seen that FSW can achieve a

steady state after several seconds. When the steady state is achieved, FSW can be treated as a quasi-static problem and then the relative velocity between the tool and the welding plate becomes a constant (but it is usually not zero). This is the heat generation nature when the classical Coulomb friction law is used in FSW simulation.

In a modified Coulomb friction law, the critical friction stress is calculated as follows,

$$\tau_{\text{crit}} = \min\left(\mu P, \sigma_{\text{s}}/\sqrt{3}\right) \qquad (6)$$

It is obvious that the friction stress in Eq. 6 is usually equal to or smaller than the one in Eq. 4.

To know the effect of the change of contact models on heat generations, four cases under lower and higher angular

Fig. 1 Temperature distributions in 350 r/min when classical Coulomb friction law is used
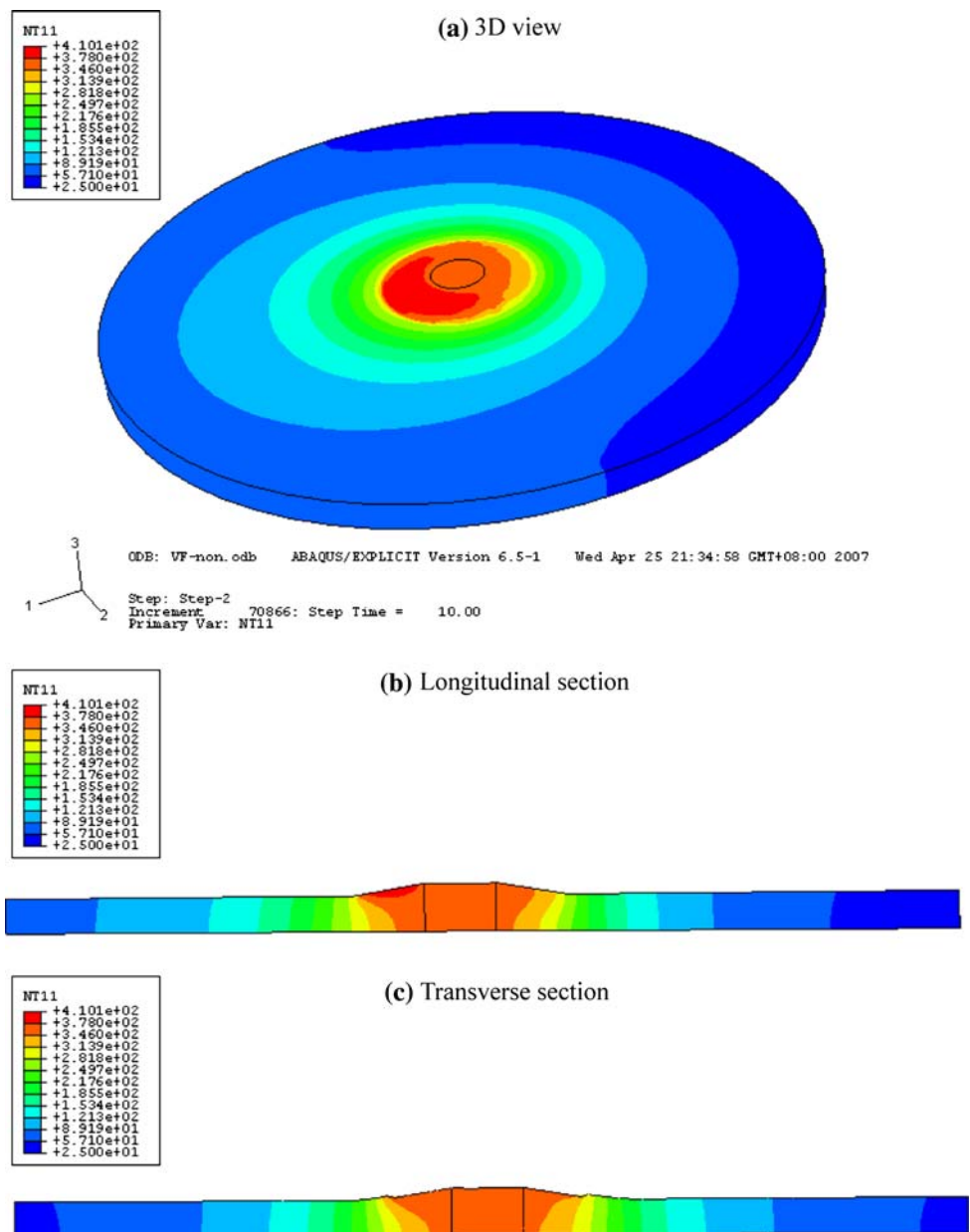
velocities are given for comparisons of the two contact models to predict the temperature and material behaviors.

Except for the friction contribution to heat generation, plastic deformation can have obvious effect on the temperature rise in FSW,
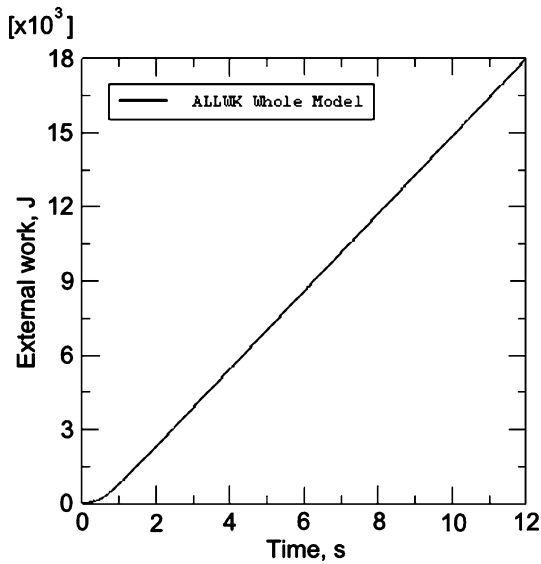
$$D_{\text{plas}} = \xi\sigma\dot{\varepsilon}_{\text{p}} \tag{7}$$

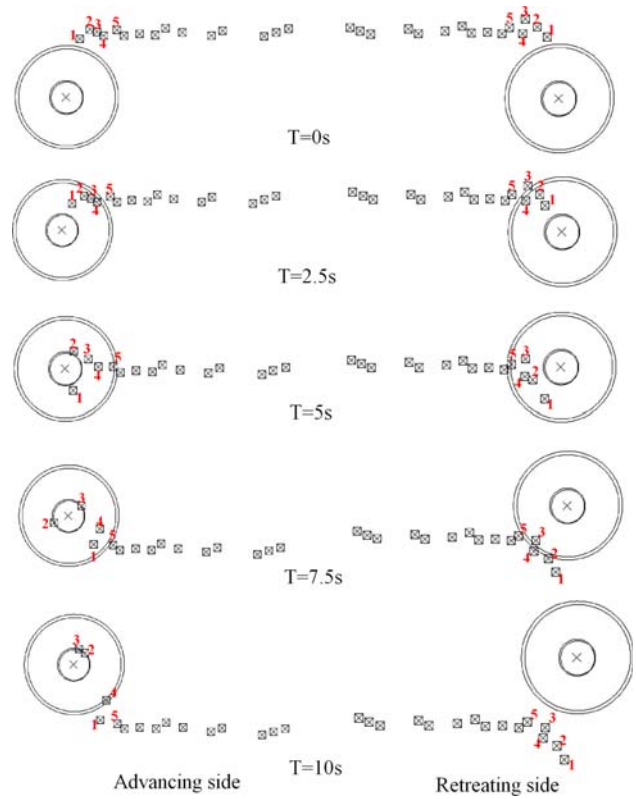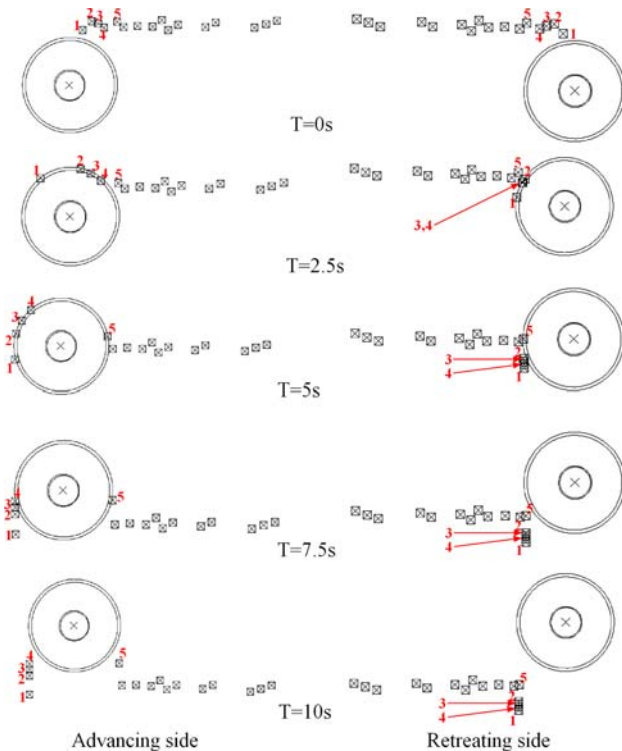Fig. 2 External work in 350 r/min when classical Coulomb friction law is used

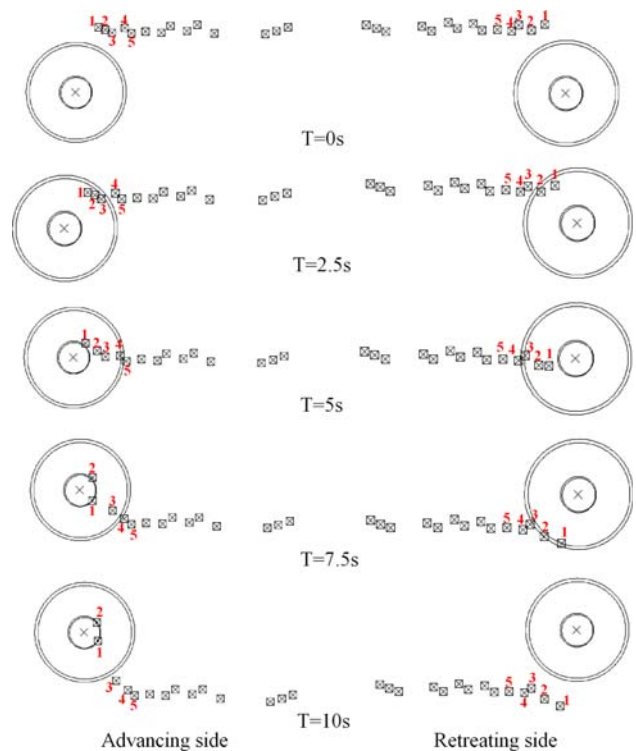Fig. 3 Material flow on the top surface in 350 r/min when classical Coulomb friction law is used

Fig. 4 Material flow in the middle of the welding plate in 350 r/min when classical Coulomb friction law is used

Fig. 5 Material flow on the bottom surface in 350 r/min when classical Coulomb friction law is used

where $\dot{\varepsilon}_p$ is the rate of equivalent plastic strain. ξ represents the fraction which is transformed into heat. Detailed description on the penalty contact algorithm can be found in Refs. [26, 27].

Results and discussions

Case 1: lower rotating speed: 350 r/min

The maximum temperature in $\omega = 350$ r/min when the classical Coulomb friction law is used is 410.1 °C, as shown in Fig. 1. Compared with the case when $\omega = 390$ r/min [21], the maximum temperature is decreased by 8.1 °C. From Fig. 1b it can be seen that the temperature

gradient in the leading edge is higher than the one in the trailing edge. The temperature in the transverse section, which is perpendicular to the welding line, is shown in Fig. 1c. Compared with the microstructure regions in the transverse section [28], it can be seen that the temperature contours can be fitted well with the boundaries of the microstructure regions, including the nugget zone, the thermo-mechanical-affected zone, and the heat-affected zone. This means that the temperature plays a key role in the microstructural evolutions. This is the reason for the temperature investigations by many researchers in the field of FSW.

According to Ref. [21], FSW can reach the steady state after several seconds. This means that the input power needed for FSW can be constant in the FSW process. This

Fig. 6 Temperature distributions in 350 r/min when modified Coulomb friction law is used
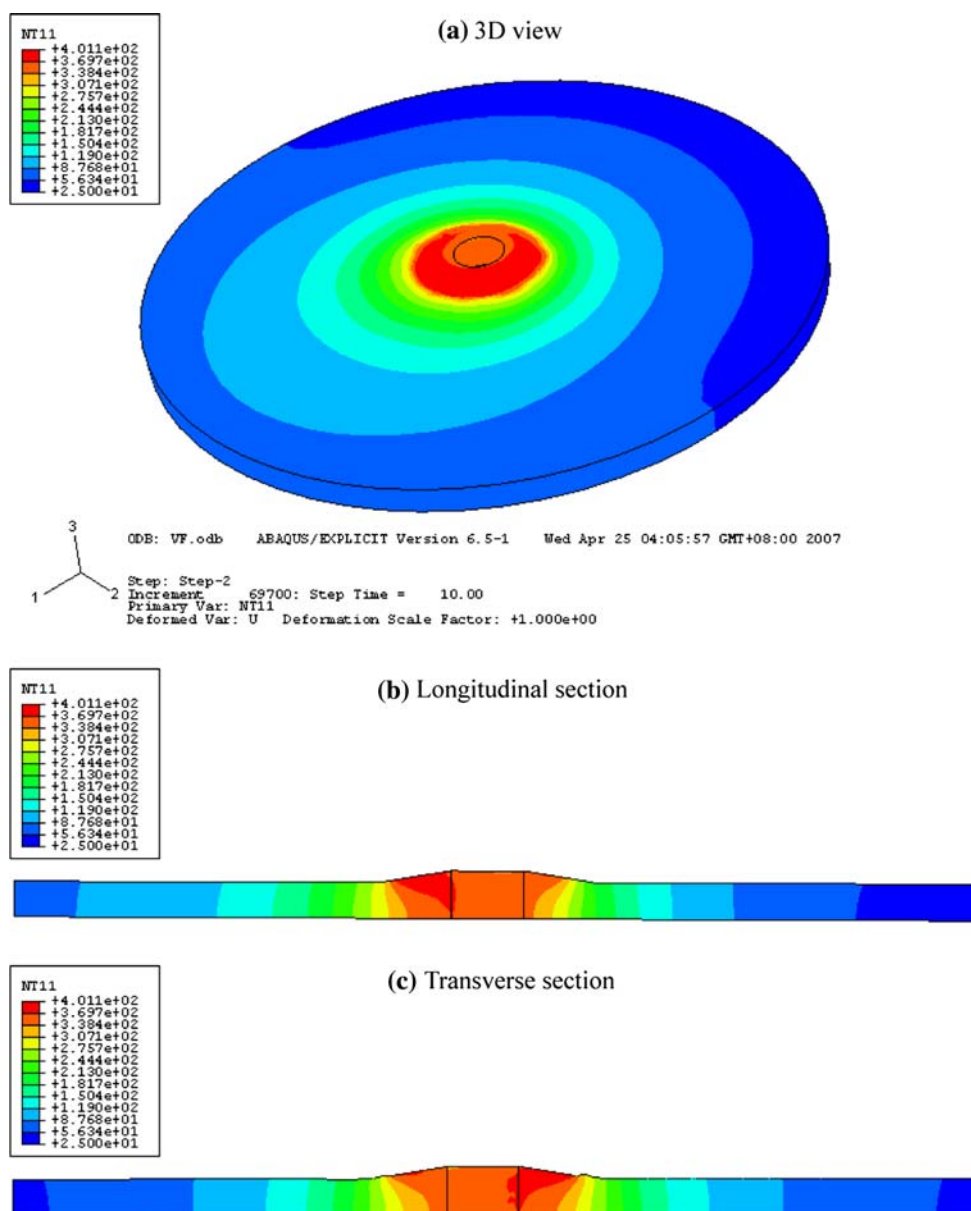
is validated in Fig. 2, which shows the relation between the external work on FSW system and time. External work is increased linearly with time.
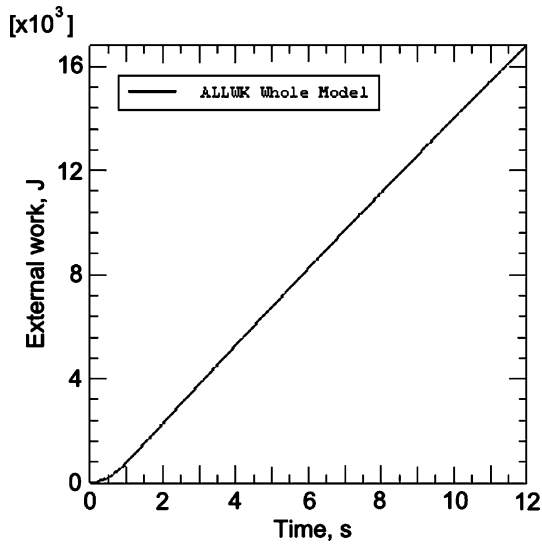

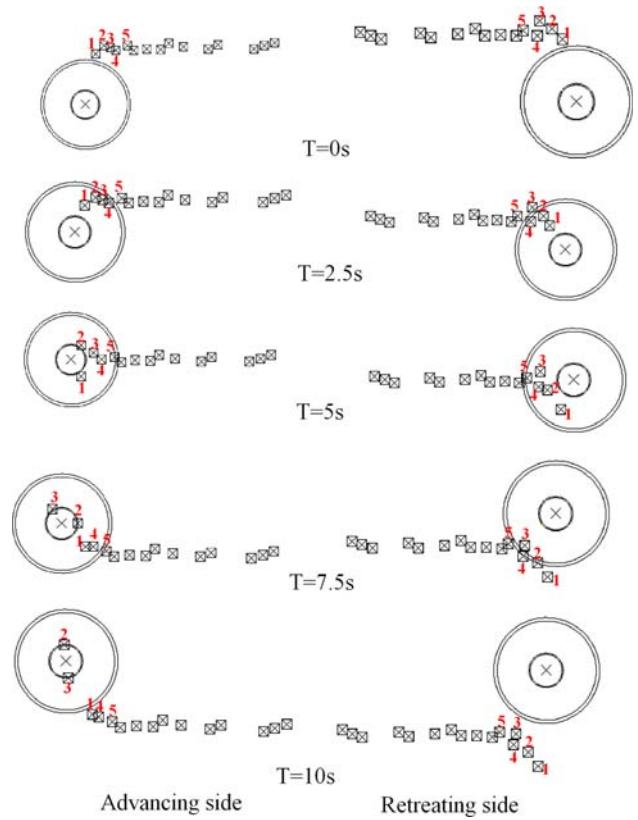Fig. 7 External work in 350 r/min when modified Coulomb friction law is used

Fig. 8 Material flow on the top surface in 350 r/min when modified Coulomb friction law is used

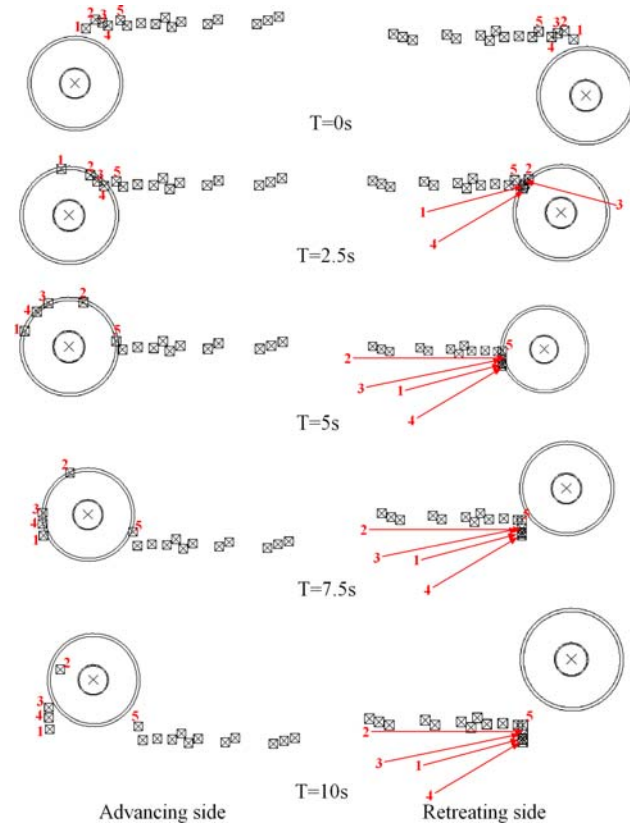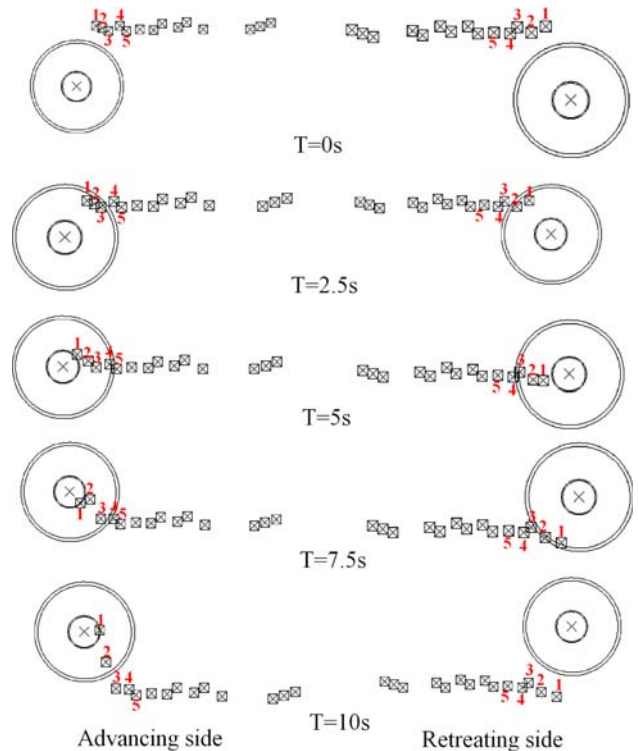Fig. 9 Material flow in the middle of the welding plate in 350 r/min when modified Coulomb friction law is used

Fig. 10 Material flow on the bottom surface in 350 r/min when modified Coulomb friction law is used

Material flow patterns are given in Figs. 3–5 to show the different material transportations in different thicknesses of the welding plate. Due to the relative smaller movements of material particles in the direction of thickness [21], the transportation of material particles in the direction of thickness is not considered for comparisons. Detailed information on material transportations can be found in Refs. [21, 22]. From Fig. 3, it can be seen that material particles on the top surface can be rotated by the border of the shoulder and deposited on the retreating side. This may be the reason for the formation of the weld flash on the retreating side in FSW.

To show the difference when the contact models are different, the temperature field in 350 r/min when modified Coulomb law is used is shown in Fig. 6. The maximum temperature is decreased to 401.1 °C. The decrease of predicted temperature is due to the decrease of the frictional stress in the tool–plate interface. Compared with the case when the classical Coulomb friction law is used, the temperature distribution under the shoulder becomes more uniform. This is because the friction stress on the interface is limited by a relatively definite value $\sigma_s(T)/\sqrt{3}$ instead of the multiplication of the friction coefficient and the solution-dependent contact pressure calculated in the classical Coulomb friction model.

The calculated external work applied on the FSW system is shown in Fig. 7 when the modified Coulomb friction law is used. Except for the initial start of FSW, the external work on the FSW system in this simulation is increased linearly with the increase of time. Based on this figure, the power needed for this model is 1.4 kW, which is slightly smaller than the model in which the classical Coulomb friction law is used.

The predicted material flows when the modified Coulomb friction law is used are shown in Figs. 8–10. Compared with the case in which the classical Coulomb friction law is used, the material behaviors are not obviously changed. But on the bottom surface, one material particle (No. 1) is rotated with the welding tool in Fig. 10, but two material particles (Nos. 1 and 2) are rotated in Fig. 5 on the advancing side at $t = 10$ s. This means that the predicted stirring effect of the welding tool when the classical Coulomb friction law is used is more obvious than the one when the modified Coulomb friction law is used, which may be caused by the decrease of friction stress on the tool–plate interface in the latter model.

From the above discussions it can be seen that the predicted temperature, efficient power, and even the material flows in the two contact models are very similar when the angular velocity is relatively small. But when the angular velocity of the welding tool is increased to a higher level, the inertia effect of the rotation of the material particles around the welding tool will become more obvious. This
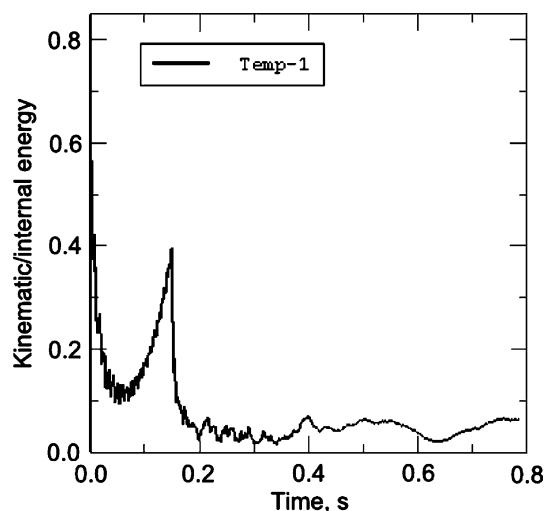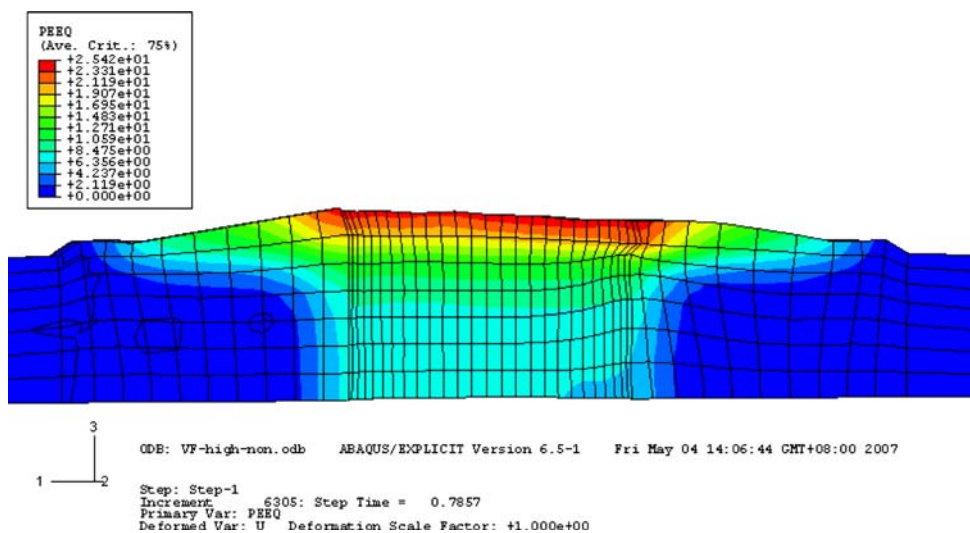

Fig. 12 Kinematic/internal energy in 1,400 r/min when classical Coulomb friction law is used

Fig. 11 Material deformation in 1,400 r/min when classical Coulomb friction law is used

can lead to the failure of the use of mass scaling factor 10^7 in the current simulation. The premise of using mass scaling is that the simulated problem must be kept quasi-static. That is, the dynamic effect cannot be much obvious. To study the differences of the two contact modes in simulating FSW in higher angular velocity, two numerical examples are added, in which the angular velocity of the welding tool is 1,400 r/min.

Case 2: higher rotating speed: 1,400 r/min

When the mass scaling factor is kept as 10^7, both the two contact models fail to complete the simulation. So, the mass scaling factor is decreased to 10^6. The material

deformation when the classical Coulomb law is used is shown in Fig. 11. It can be seen that the simulation cannot be continued due to excessive deformations on the tool–plate interface, which is caused by the dynamic effect due to the use of mass scaling, as shown in Fig. 12.

When the modified contact model is used, the simulation can be continued. This is because the decrease of the frictional stress on the tool–plate interface leads to the decrease of the dynamic effect caused by the welding tool. The temperature field obtained in this contact model in 1,400 r/min is shown in Fig. 13. Compared with the case in 350 r/min, the maximum temperature is increased from 401.1 to 441.5 °C. Although the increase of the angular velocity is very obvious, the increase of the maximum

Fig. 13 Temperature distributions in 1,400 r/min when modified Coulomb friction law is used
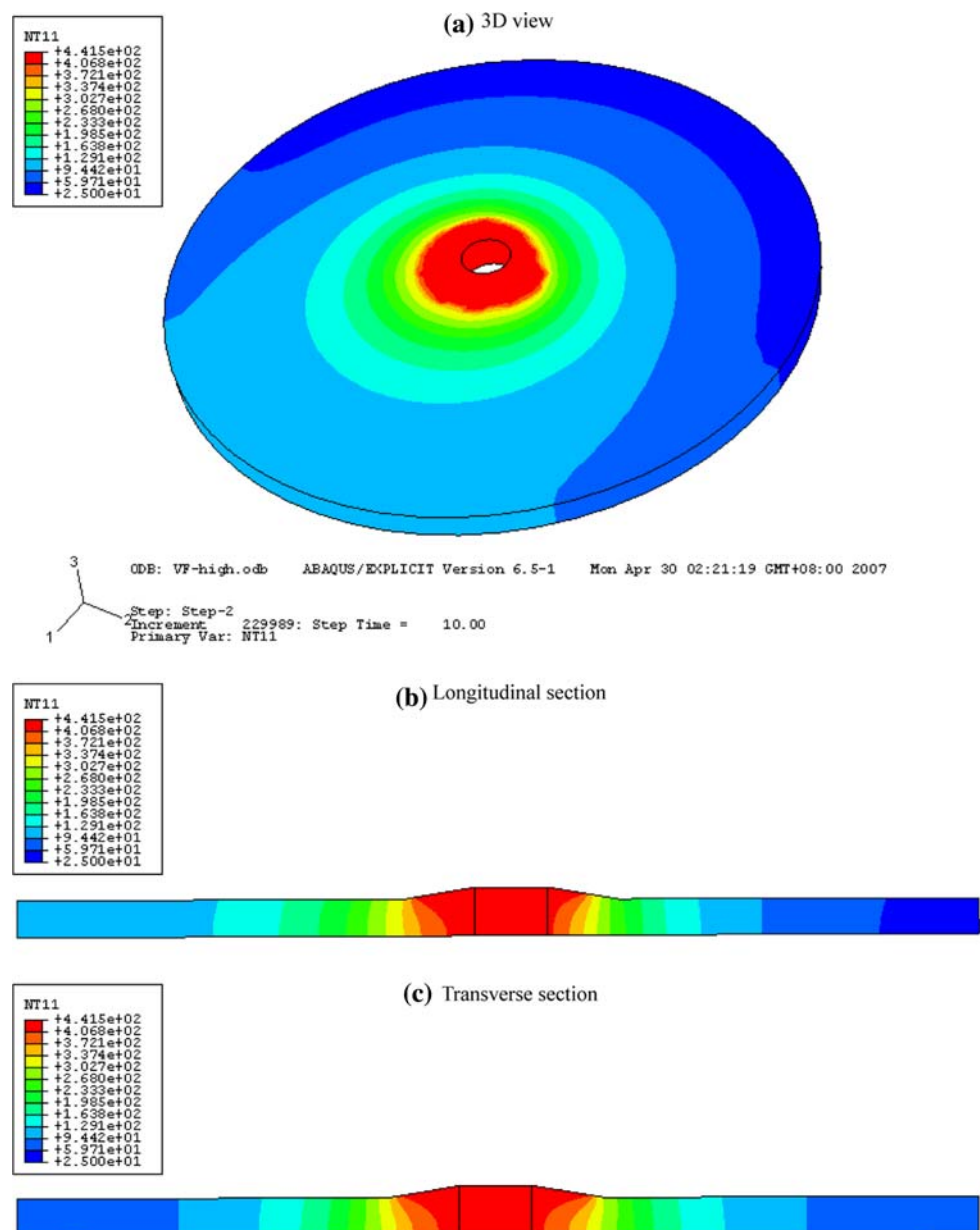
temperature is relatively smaller. This means that FSW can be kept as a solid state joining technology even in a wide range of variation of angular velocity.

From the above discussions, it can be concluded that the limitation caused by the shear failure of the welding material to the upper limit of the frictional stress on the
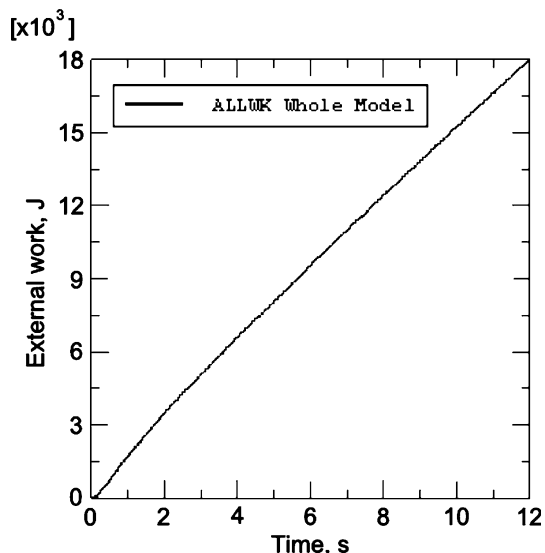

Fig. 14 External work in 1,400 r/min when modified Coulomb friction law is used
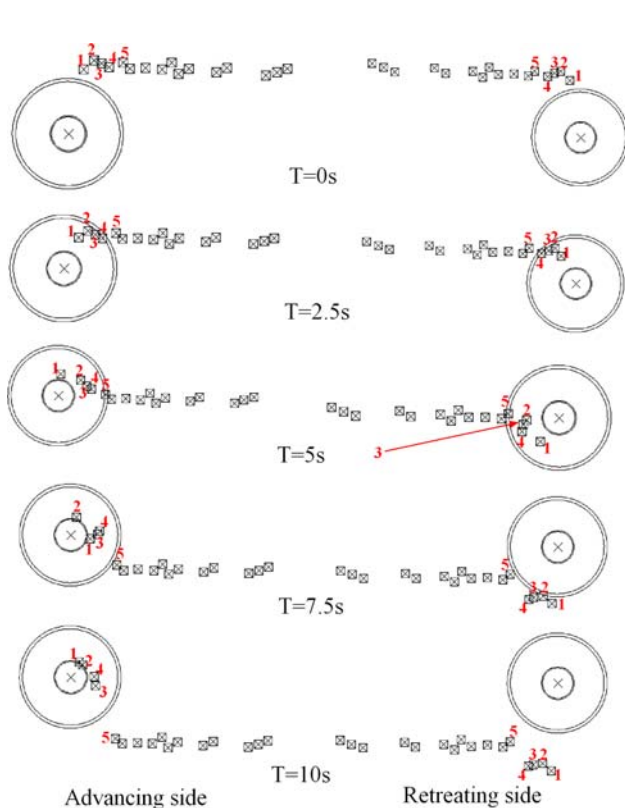
tool–plate interface is the real reason for the solid state nature of FSW. This means that the modified contact model is more realistic for the simulation of FSW. But when the angular velocity of the welding tool is lower, the two models do not show obvious difference. This means that the effect of the contact model is very small in lower angular velocity, but is very obvious in higher angular velocity, which should be noted in the simulation of FSW by researchers.

The external work on the FSW system calculated in this simulation is shown in Fig. 14. The input power is increased from 1.4 kW in 350 r/min to 1.5 kW in 1,400 r/min. The increase of the angular velocity leads to the increase of the efficient input power of FSW machine.

When the angular velocity is very high, the material transportations are obviously different from the case in lower angular velocity. In lower angular velocity, the material particles on the top surface do not enter into the region under the shoulder, which can lead to the formation of weld flash in FSW. The weld flash is not desirable and needs to be carefully controlled. When the angular velocity is increased to 1,400 r/min, the material particles can enter into the region under the shoulder and do not deposit on the border of the shoulder at the retreating side, as shown in Figs. 15 and 16. In lower angular velocity, the material particles on the bottom
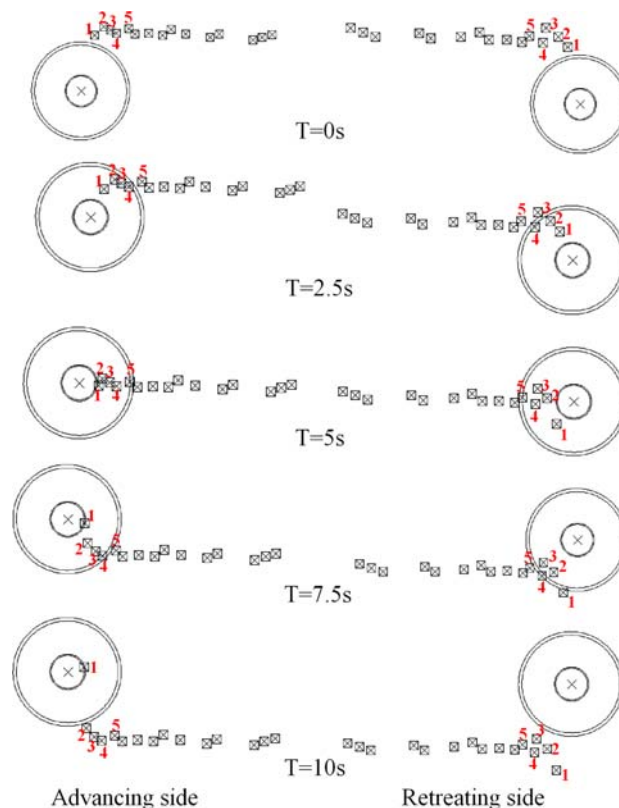

Fig. 15 Material flow on the top surface in 1,400 r/min when modified Coulomb friction law is used

Fig. 16 Material flow in the middle of the welding plate in 1,400 r/min when modified Coulomb friction law is used
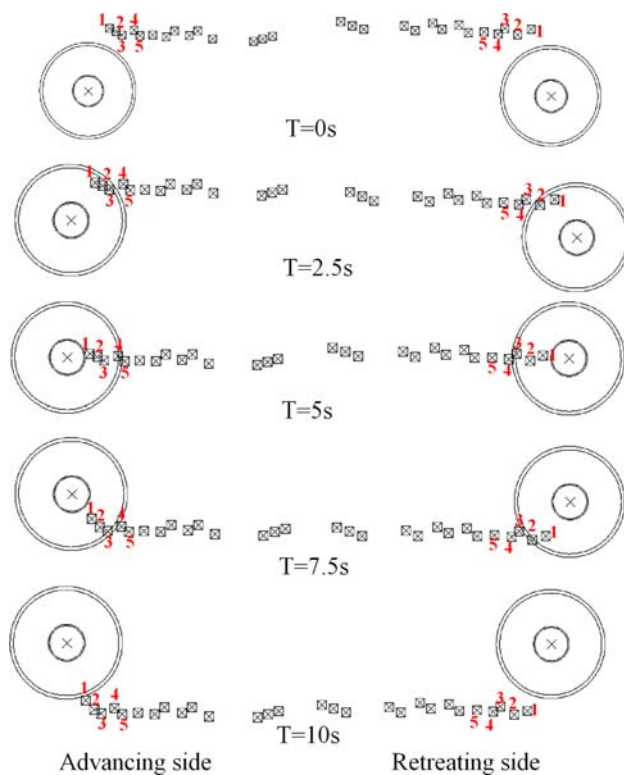
Fig. 17 Material flow on the bottom surface in 1,400 r/min when modified Coulomb friction law is used

surface can be mixed due to the rotation of the welding tool. The material particles at the advancing side can be rotated with the welding tool but this phenomenon cannot be seen in Fig. 17, which will lead to the relative decrease of the joint strength compared with the other parts in higher angular velocity. From the above discussion it can be seen that the mechanical properties of the joint can be relatively decreased on the bottom surface compared with the top surface with the increase of the angular velocity of the welding tool. This means that the differences of the mechanical properties on the top and bottom surfaces can become increased with the increase of the angular velocity. In Ref. [28], it can also be seen that the differences in material velocities become increased with the increase of the angular velocity of the welding tool, but the decrease of joint strength cannot be shown in Ref. [28] due to the neglect of the heat generation in that semi-coupled thermo-mechanical analysis. The comparison shows the current model with consideration of shear failure criteria is more realistic.

Remark

Experiments on FSW also show that the mechanical properties of friction stir weld in different thicknesses are different [29, 30], which is caused by the different dynamic recrystallization in friction stir weld [31]. In fact, the

evolution of grain size can be related to the plastic deformation and the temperature in FSW [32]. With consideration of the grain size evolution model used in Ref. [32], the grain size can be increased with the increase of the temperature in FSW and the decrease of the plastic strain and strain rate. The quantitative analysis of the grain size evolution is strongly dependent on the determination of the material constants by experiments and the computational results of the temperature and the plastic deformation by numerical tests.

Conclusions

Two contact models, including the classical Coulomb friction law and the modified Coulomb friction law in which the upper limit of friction stress is determined by the shear failure, are combined with a fully coupled thermo-mechanical model for comparisons in the simulation of friction stir welding. The obtained results are summarized as follows,

(1) In lower angular velocity, the two contact models do not show obvious differences in the simulation of FSW in the temperature prediction and the prediction of the material transportations. But in higher angular velocity, the classical Coulomb friction law fails to complete the simulation due to the increase of the dynamic effect of the welding tool.

(2) The material particles are rotated by the border of the shoulder and cannot enter into the region under the shoulder in lower angular velocity, which is the reason for the formation of the weld flash.

References

1. Thomas WM, Nicholas ED, Needham JC, Murch MG, Templesmith P, Dawes CJ (1991) Friction stir welding, International Patent Application No. PCT/GB92102203 and Great Britain Patent Application No. 9125978.8
2. Squillace A, De Fenzo A, Giorleo G, Bellucci F (2004) J Mater Process Technol 152:97. doi:10.1016/j.jmatprotec.2004.03.022
3. Reynolds AP, Tang W, Khandkar Z, Khan JA, Lindner K (2005) Sci Technol Weld Join 10(2):190. doi:10.1179/174329305 X37024
4. Colegrove PA, Shercliff HR (2003) Sci Technol Weld Join 8(5):360. doi:10.1179/136217103225005534

5. Chen CM, Kovacevic R (2004) Int J Mach Tools Manuf 44:1205. doi:10.1016/j.ijmachtools.2004.03.011

6. David SA, DebRoy T (1992) Science 257:497. doi:10.1126/science.257.5069.497

7. Khandkar MZH, Khan JA, Reynolds AP (2003) Sci Technol Weld Join 8(3):165. doi:10.1179/136217103225010943

8. Mandal S, Williamson K (2006) J Mater Process Technol 174:190. doi:10.1016/j.jmatprotec.2005.12.012

9. Bastier A, Maintournam MH, Dang Van K, Roger F (2006) Sci Technol Weld Join 11(3):278. doi:10.1179/174329306X102093

10. Song M, Kovacevic R (2003) Int J Mach Tools Manuf 43:605. doi:10.1016/S0890-6955(03)00022-1

11. Schmidt H, Hattel J (2005) Model Simul Mater Sci Eng 13:77. doi:10.1088/0965-0393/13/1/006

12. Guerra M, Schmidt C, McClure JC, Murr LE, Nunes AC (2003) Mater Charact 49:95. doi:10.1016/S1044-5803(02)00362-5

13. Colligan K (1999) Weld Res, Suppl Weld J:229

14. Li Y, Murr LE, McClure JC (1999) Mater Sci Eng A 271:213. doi:10.1016/S0921-5093(99)00204-X

15. Muthukumaran S, Mukherjee SK (2006) Sci Technol Weld Join 11(3):337. doi:10.1179/174329306X107665

16. Reynolds AP (2000) Sci Technol Weld Join 5(2):120. doi:10.1179/136217100101538119

17. Buffa G, Hua J, Shivpuri R, Fratini L (2006) Mater Sci Eng A 419:389. doi:10.1016/j.msea.2005.09.040

18. Nandan R, Roy GG, Lienert TJ, Debroy T (2007) Acta Mater 55:883. doi:10.1016/j.actamat.2006.09.009

19. Zhang HW, Zhang Z, Chen JT (2005) Mater Sci Eng A (403):340. doi:10.1016/j.msea.2005.05.052

20. Zhang HW, Zhang Z, Chen JT (2007) J Mater Process Technol 183:62. doi:10.1016/j.jmatprotec.2006.09.027

21. Zhang Z, Zhang HW (2008) Int J Adv Manuf Technol 37:279. doi:10.1007/s00170-007-0971-6

22. Zhang Z, Zhang HW (2007) Sci Technol Weld Join 12(3):226. doi:10.1179/174329307X177919

23. Nandan R, Roy GG, Lienert TJ, DebRoy T (2006) Sci Technol Weld Join 11(5):526. doi10.1179/174329306X107692i:

24. Feng AH, Ma ZY (2007) Scr Mater 56:397. doi:10.1016/j.scriptamat.2006.10.035

25. Ma ZY, Sharma SR, Mishra RS (2006) Mater Sci Eng A 433:269. doi:10.1016/j.msea.2006.06.099

26. Zhang HW, Zhong WX, Wu CH, Liao AH (2006) Int J Mech Sci 48:176. doi:10.1016/j.ijmecsci.2005.08.003

27. Zhang HW, Wang H, Wriggers P, Schrefler BA (2005) Comput Mech 36(6):444. doi:10.1007/s00466-005-0680-7

28. Zhang Z, Zhang HW (2007) Int J Adv Manuf Technol 35:86. doi:10.1007/s00170-006-0707-z

29. Liu HJ, Fujii H, Maeda M, Nogi K (2003) J Mater Sci Lett 22:441. doi:10.1023/A:1022959627794

30. Lin SB, Zhao YH, Wu L (2006) Mater Sci Technol 22(8):995. doi:10.1179/174328406X102408

31. Murr LE, Liu G, McClure JC (1997) J Mater Sci Lett 16:1801. doi:10.1023/A:1018556332357

32. Fratini L, Buffa G (2005) Int J Mach Tools Manuf 45:1188. doi:10.1016/j.ijmachtools.2004.12.001